Available online at www.sciencedirect.com

SciVerse ScienceDirect

Ceramics International 38 (2012) 1381–1390

CERAMICS INTERNATIONAL

www.elsevier.com/locate/ceramint

Plastic behaviour of 4H–SiC single crystals deformed at temperatures between 800 and 1300 °C

A. Lara, A. Muñoz *, M. Castillo-Rodríguez, A. Domínguez-Rodríguez

Departamento de Física de la Materia Condensada, Facultad de Física, Universidad de Sevilla, Apartado 1065, 41012 Sevilla, Spain

Received 30 July 2011; received in revised form 6 September 2011; accepted 7 September 2011
Available online 17 September 2011

Abstract

We studied the mechanical behaviour of 4H–SiC single crystals tested under compression at temperatures between 800 °C and 1300 °C. The tests were conducted at a constant strain rate ($\dot{\varepsilon} = 1.5 \times 10^{-5}$ s^{-1} and $\dot{\varepsilon} = 3.0 \times 10^{-5}$ s^{-1}) and constant load (creep) in a stress range between 28 and 110 MPa. Transmission electron microscopy (TEM) observations allowed us to correlate the results of the mechanical tests with the dislocation microstructure of deformed specimens. Both the mechanical results and the TEM observations revealed the existence of a change in deformation mechanisms at a critical temperature $T_c \sim 1000$ °C. The parameters characterizing the deformation mechanisms – the stress exponent and the activation energy – were evaluated from the mechanical tests at temperatures above and below T_c. The value obtained for the stress exponent was $n = 2.8 \pm 0.8$ in the tests at constant strain rate and $T > T_c$, and $n = 2.9 \pm 0.3$ in the creep tests over the entire temperature range. The constant strain rate tests gave activation energies of $Q = 0.7 \pm 0.3$ eV for $T < T_c$ and $Q = 3.3 \pm 0.6$ eV for $T > T_c$, and the corresponding values given by the creep tests were between $Q = 1.4 \pm 0.1$ eV and $Q = 2.3 \pm 0.6$ eV for $T < T_c$, and $Q = 3.5 \pm 0.7$ eV for $T > T_c$. The TEM observations showed that at $T > T_c$ most basal dislocations were dissociated into two partial dislocations that glide simultaneously, leaving only a small stacking fault γ between them. In contrast to this behaviour, at $T < T_c$ the deformation takes place by the glide of just one of the partials-that of lower activation energy (leading partial) with a core of Si atoms, without the twin partial of higher activation energy (trailing partial) and C atom core having been nucleated. The glide of the leading partial leaves behind it a large stacking fault zone of the glide plane. In both temperature ranges, the slip traces are long and straight along simple crystallographic directions, suggesting that the movement of the dislocations is controlled by the Peierls mechanism over the entire temperature range studied. The results of the mechanical tests, together with optical microscopy of the lateral faces of the deformed specimens and TEM observations are used as a basis for an analysis and discussion of the most significant features of the plasticity of the material and of the deformation mechanisms operating in the two temperature ranges.

Keywords: B. Electron microscopy; C. Mechanical properties; C. Creep; D. SiC

1. Introduction

The advanced ceramic SiC is currently of great interest due to its excellent physicochemical properties such as resistance to erosion and corrosion, high thermal conductivity, small expansion coefficient, low density, and hardness second only to diamond. This polycrystalline material is widely used in industry as an abrasive (grinding, sanding, etc.), for refractory products (bricks, crucibles, etc.), and as a structural material in the manufacture of such products as bearings, valves, resistors, etc. Moreover, recent advances providing precise knowledge of its crystal structure together with developments in the physics of electronics endow this material with a promising future in functional applications as well. In particular its properties as a wide band gap semiconductor make it a good candidate for the manufacture of electronic devices that are operative at high temperatures and in harsh environments – conditions under which it is impossible to use other semiconductor materials such as Si or GaAs. The crystallographic structure of SiC based on the tetrahedral coordination of C and Si atoms leads to the formation of different polytypes resulting from the distinct spatial arrangements of these tetrahedra. The deformation of SiC single crystals by partial dislocations gives rise to stacking faults that modify these arrangements and transform one

* Corresponding author. Tel.: +34 954550939; fax: +34 954552870.
E-mail address: anmube@us.es (A. Muñoz).

0272-8842/$36.00
doi:10.1016/j.ceramint.2011.09.017

polytype into another. This affects not only the mechanical but also the semiconducting properties of the material. It is therefore important to understand the deformation mechanisms of SiC single crystals, and to study the structural changes that these mechanisms give rise to in different polytypes. While the plasticity of many semiconductor materials has been extensively studied over a wide range of stresses and temperatures [1,2], there is still a certain lack of data on the plastic deformation of the different polytypes of SiC. This is mainly due to the difficulty of growing these crystals to a large enough size for mechanical testing. Indeed, it was not until the end of the last century that these crystals began to be commercially available [3].

The first experiments on the plasticity of SiC in single crystals were performed by Fujita et al. [4] with small specimens of industrially grown 6H–SiC crystals. These uniaxial compression tests involved basal gliding at a constant strain rate for temperatures between 1100 °C and 1800 °C. Later Samant et al. [5] performed experiments with 6H–SiC, and observed a change in the deformation mechanism at temperatures around 1100 °C. Their TEM observations of the dislocation microstructure of deformed specimens at temperatures above 1100 °C showed the presence of the dissociation into two partial basal dislocations, according to the equation:

$$\frac{1}{3}\langle \bar{1}\,2\,\bar{1}\,0\rangle \rightarrow \frac{1}{3}\langle \bar{1}\,1\,0\,0\rangle + \frac{1}{3}\langle 0\,1\,\bar{1}\,0\rangle \quad (1)$$

Below this temperature, only one of the partials was observed, together with the existence of large areas of stacking faults. Subsequently, Samant and Pirouz [6] and Demenet et al. [7] observed a similar transition in the 4H–SiC deformation mechanisms, and determined a value for the transition temperature between 1030 °C and 1100 °C, depending on the strain rate. Finally, Demenet et al. [8] analyzed the microstructure dislocations in 4H–SiC deformed at very high stresses (up to 5 GPa) and low temperatures ($T \leq 1350$ °C). Their TEM observations showed that, under these conditions, deformation is possible by the glide of undissociated basal dislocations.

The deformation of SiC single crystals by partial dislocation glide gives rise to the transformation of one polytype into another. Pirouz and Yang [9] proposed a model for these transformations based on the different mobility of the partial dislocations originating from the dissociation of the perfect basal dislocation. This difference in mobility is attributed to the differing composition of the core of the two partial dislocations.

The aim of the present work is to contribute to understanding the mechanisms of deformation by basal glide of 4H–SiC by adding to the literature's currently rather sparse experimental data on the plastic deformation of this polytype. To this end, compression tests were performed at constant strain rates ($\dot{\varepsilon} = 1.5 \times 10^{-5}$ s^{-1} and $\dot{\varepsilon} = 3.0 \times 10^{-5}$ s^{-1}) and a wide range of temperatures. Such experiments are not, however, the most appropriate for determining the parameters that characterize the deformation mechanisms – the stress exponent and the activation energy. For the determination of these parameters, we conducted creep tests at constant load over a wide stress range (between 28 and 110 MPa) and at temperatures between 900 °C and 1250 °C. There have been no previously reported data from creep tests referring to 4H–SiC. There is only creep data for the 6H–SiC polytype published by Corman [10]. Based on the results of the present mechanical tests and the transmission electron microscopy (TEM) observations of the deformed specimens we shall discuss the different deformation mechanisms operating in each temperature range.

2. Experimental procedure

The crystals used in this work were provided by *Sterling Semiconductor, Inc. (USA)* as cylinders 5 cm in diameter, grown by the physical vapour transport (PVT) technique along the [0 0 0 1] direction. The as-received crystals were oriented using the Laue X-ray back-reflection technique. The specimens for mechanical tests were cut in the form of parallelepipeds of 2.7 mm × 2.7 mm × 5.5 mm using a low-speed diamond saw. They were oriented to favour the activation of only one $(0\,0\,0\,1)(1/3)\langle \bar{1}\,2\,\bar{1}\,0\rangle$ basal slip system with a Schmid factor of $f_s = 0.5$. Fig. 1 shows this orientation in which two lateral faces of the sample are parallel to the $\{\bar{1}\,0\,1\,0\}$ plane. The compression axis lies in this plane, at 45° from the [0 0 0 1] direction. In order to allow optical observations of the slip traces at the surface after straining, the specimens were polished with diamond pastes down to 3 μm in grain size.

Deformation tests were performed in air at temperatures between 800 °C and 1300 °C at cross-head speeds of 5 and 10 μm min^{-1}, corresponding to initial strain rates of ($\dot{\varepsilon} = 1.5 \times 10^{-5}$ and $\dot{\varepsilon} = 3.0 \times 10^{-5}$ s^{-1}) in an Instron machine, model 1185. Creep tests were performed in air at temperatures between 900 °C and 1250 °C and stresses between 28 and 110 MPa in a prototype creep machine. In both cases, the load was transmitted to the specimens via polycrystalline SiC rods. Slip traces were analyzed by optical microscopy (*Leica DMRE*).

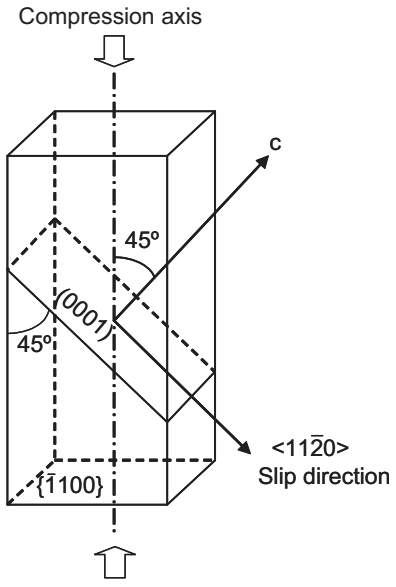

Fig. 1. Orientation of the samples for mechanical tests, indicating the slip plane and direction.

Foils parallel to basal plane (0 0 0 1) were cut from deformed samples for transmission electron microscopy (TEM) observation. This orientation provides a suitable vision of the dislocation microstructure because it is possible to observe dislocations along some dozens of microns and allows acquiring a sufficiently precise idea on the organization and the ways of expansion of dislocations. The foils were mechanically ground to a thickness of about 100 μm and polished with diamond paste of grain size down to 3 μm. Then they were dimpled to ∼30 μm (*Dimpler grinder Gatan Model-656*) and ion beam thinned to electron transparency (*PIPS Gatan Model-691*). A thin carbon coat was deposited on the foils by vacuum evaporation to prevent charge buildup during observation in the electron microscope. The Burgers vectors of basal dislocations and partials, in case of dissociation, were determined with standard **g**·**b** analysis. The specimens were examined by the *weak beam* technique, which is more suitable than conventional TEM techniques to study dislocation fine structure, using a Philips CM 200 microscope operating at 200 kV.

3. Results

3.1. Deformation tests at constant strain rate

These tests were carried out at temperatures between 800 °C and 1300 °C and an initial strain rate of $\dot{\varepsilon} = 1.5 \times 10^{-5}\ \text{s}^{-1}$. In the trials at $T \geq 1000$ °C, at deformations close to 4% (once past the yield point) the strain was jumped up to $3.0 \times 10^{-5}\ \text{s}^{-1}$ to evaluate the stress exponent n characteristic of the deformation mechanism. Fig. 2 shows the resulting stress–strain curves. The significant change one observes in the shape of these curves for temperatures around 1000 °C is indicative of the existence of some change in the deformation mechanisms. At $T \geq 1100$ °C, the stress–strain curves show the typical behaviour of a single crystal deformed by the activation of a glide system, with a greater value of the upper point the lower the temperature. This reflects the need for greater stresses to activate the generation and propagation of dislocations at lower temperatures. After the yield point, the deformation stress decreases with increasing temperature, reflecting the greater ease of movement of the dislocations after their generation and after the necessary adjustments in their slip speed. There was no significant work hardening, indicating that the processes of interaction between dislocations play no major role in the deformation, at least at the strains we were working with ($\varepsilon < 10\%$). At $T \leq 900$ °C, the behaviour of the stress-strain curves is different. The yield point has gone, implying a greater difficulty to activate the mechanisms of multiplication of dislocations, so that there will be no avalanche in the density of mobile dislocations. In this case, one observes a slight work hardening from the beginning of the deformation. The stress–strain curve for $T = 1000$ °C shows a behaviour intermediate between those described above, so that the different mechanisms must each have contributed in some proportion to the deformation of the material at this temperature. However, observation of the slip traces on the lateral faces of the deformed specimens shows that in all cases the deformation takes place by activation of basal glide.

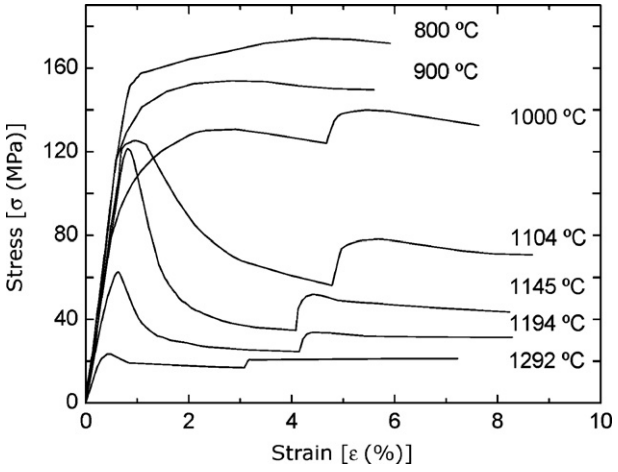

Fig. 2. Stress–strain curves of the 4H–SiC samples deformed at temperatures between 800 °C and 1300 °C at a strain rate of $\dot{\varepsilon} = 1.5 \times 10^{-5}\ \text{s}^{-1}$. For $T \geq 1000$ °C, the strain rate was jumped up to $\dot{\varepsilon} = 3.0 \times 10^{-5}\ \text{s}^{-1}$ until $\varepsilon \sim 4\%$.

The generally accepted expression for the strain rate in covalent crystals deformed by dislocation glide is [11,12]:

$$\dot{\varepsilon} = A\,\tau_c^n \exp\left(\frac{-Q}{kT}\right) \tag{2}$$

where A is a constant, $\tau_c = \sigma \times f_s$ is the critical resolved stress measured at the lower point, n the stress exponent, Q the activation energy for dislocation glide, T the absolute temperature, and k Boltzmann's constant. Assuming that Q is independent of the strain rate and applied stress, the stress exponent n can be obtained as

$$n = \left(\ln\frac{\dot{\varepsilon}_1}{\dot{\varepsilon}_2}\bigg|_T\right) \cdot \left(\ln\frac{\tau_{c1}}{\tau_{c2}}\bigg|_T\right)^{-1} \tag{3}$$

The values of the critical resolved stress τ_c for each temperature and each strain rate are given in Table 1. Also given are the values of n obtained from the strain rate jump tests performed at $T \geq 1000$ °C, according to Eq. (3). The estimated average value for the stress exponent from these experiments is $n = 2.8 \pm 0.8$ at $T \geq 1000$ °C.

Considering the activation energy for dislocation movement to be independent of temperature and of the applied stress, one

Table 1
Critical resolved stress values τ_c for different temperatures and two values of the strain rate $\dot{\varepsilon}_1$ and $\dot{\varepsilon}_2$, together with the values of the stress exponent n obtained for $T \geq 1000$ °C.

T (°C)	τ_c (MPa)		n
	$\dot{\varepsilon}_1 = 1.5 \times 10^{-5}\ \text{s}^{-1}$	$\dot{\varepsilon}_2 = 3.0 \times 10^{-5}\ \text{s}^{-1}$	
800	86.73	–	–
900	75.46	–	–
1000	57.92	70.85	3.7
1104	26.80	36.75	2.3
1145	17.95	25.09	2.1
1194	12.25	16.85	2.3
1292	8.35	10.35	3.4

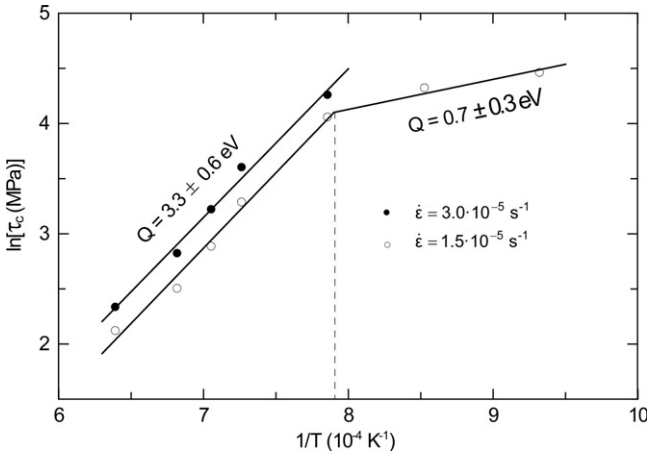

Fig. 3. Plot of ln τ_c versus $1/T$ for the basal slip in 4H–SiC at different strain rates. ●, $\dot{\varepsilon} = 3.0 \times 10^{-5}$ s^{-1}; ○, $\dot{\varepsilon} = 1.5 \times 10^{-5}$ s^{-1}.

can obtain the value of Q/n from the slope of a straight line fit to ln τ_c against $1/T$ for constant $\dot{\varepsilon}$, according to the expression:

$$\ln \tau_c = \frac{Q}{nk}\frac{1}{T} + \frac{\ln \dot{\varepsilon} - \ln A}{n} \quad (4)$$

Fig. 3 is a plot of this relationship for the entire range of temperatures at $\dot{\varepsilon} = 1.5 \times 10^{-5}$ s^{-1}, and for $T \geq 1000$ °C at $\dot{\varepsilon} = 3.0 \times 10^{-5}$ s^{-1}. The two different segments of the plot in the former case suggest the existence of two deformation mechanisms depending on the test temperature, each characterized by a different activation energy Q. At $\dot{\varepsilon} = 1.5 \times 10^{-5}$ s^{-1} the intersection of the two segments determines the temperature $T_c = 993$ °C which the change of deformation mechanism takes place.

The greater values of the resolved stresses for $\dot{\varepsilon} = 3.0 \times 10^{-5}$ s^{-1} suggest that the critical transition temperature T_c should increase with strain rate, but this was not verified in our work. It may account, however, for the slightly different values of T_c obtained by other authors [6,7,13] (Table 2).

Assuming that the value $n = 2.8 \pm 0.8$ obtained for $T \geq 1000$ °C is valid throughout that temperature range, we obtained the following activation energies from the slopes of the straight line fits in Fig. 3: $Q = 3.3 \pm 0.6$ eV at $T > T_c$ for both strain rates, and $Q = 0.7 \pm 0.3$ eV at $T < T_c$ for $\dot{\varepsilon}_1 = 1.5 \times 10^{-5}$ s^{-1}.

3.2. Compressive creep tests

Creep tests were carried out at temperatures between 900 °C and 1250 °C, with stresses between 28 and 110 MPa. The specimens were deformed to about 15% with strain rates between 10^{-6} and 10^{-4} s^{-1}. Fig. 4 shows some typical curves obtained at constant load. Fig. 4a corresponds to temperatures $T > T_c$, and Fig. 4b to temperatures $T < T_c$. They are plots of strain rate $\dot{\varepsilon}$ versus strain ε for different test temperatures and applied stresses. After a change in temperature or applied stress, the strain rate tends to a new steady state characterized by a constant value of $\dot{\varepsilon}$. Changes in the applied stress, maintaining the temperature constant, allow one to determine the stress exponent n of Eq. (2) from Eq. (3) in which the subscripts 1 and 2 correspond to the values of the applied resolved stress τ_c or of $\sigma = \tau_c/f_s$, and of the steady state value of $\dot{\varepsilon}$ before and after the stress jump. Likewise, the value of the activation energy for dislocation movement Q can be obtained from the temperature changes at constant load using the formula:

$$Q = -k\left.\frac{d\ln\dot{\varepsilon}}{d(1/T)}\right|_{\sigma} \approx -k\left(\ln\frac{\dot{\varepsilon}_2}{\dot{\varepsilon}_1}\right)\cdot\left(\frac{1}{T_2} - \frac{1}{T_1}\right)^{-1} \quad (5)$$

in which the subscripts 1 and 2 refer to the values of $\dot{\varepsilon}$ and T before and after the temperature jump. Fig. 4a and b shows the values of n and Q calculated at the different stress and temperature jumps using Eqs. (3) and (5). The mean values obtained were: $Q = 3.5 \pm 0.7$ eV for temperatures above T_c, and $Q = 2.3 \pm 0.6$ eV for temperatures below T_c; and $n = 2.9 \pm 0.3$ over the whole temperature range. These results are in good agreement with those obtained previously from compression tests at constant strain rates.

As will be discussed below, at temperatures below T_c the mechanisms that lead to deformation of the material are not very effective in achieving high strain rates. For this reason, we performed creep tests at these relatively low temperatures,

Table 2
Summary of the experimental results obtained in previous works performed at constant strain rate of the 4H–SiC and 6H–SiC single crystals.

Polytype	Reference	Strain rate $\dot{\varepsilon}$ (s^{-1})	Critical temperature T_c (°C)	Stress exponent n	Activation energy Q (eV)	
					$T < T_c$	$T > T_c$
4H–SiC	Samant et al. [6,19]	3.1×10^{-5}	1100	3.0 ± 0.8	1.8 ± 0.7	4.5 ± 1.2
		6.3×10^{-5}			2.1 ± 0.7	3.6 ± 1.2
		1.3×10^{-4}				2.1 ± 0.7
		6.5×10^{-4}				1.8 ± 0.7
	Demenet et al. [7]	2.6×10^{-6}	1030	$2.5 - 3.0$	0.25n	4.5 ± 0.3
		3.6×10^{-5}	1100		–	5.4 ± 0.6
	Pirouz et al. [13]	2.6×10^{-6}	1030			
		3.6×10^{-5}	1100			
		3.6×10^{-4}	1160			
6H–SiC	Samant et al. [6,19]	3.1×10^{-5}	1100	3.0 ± 0.8	1.8 ± 0.7	4.8 ± 1.8
		6.3×10^{-5}				2.4 ± 0.8
		1.3×10^{-4}				1.8 ± 0.7
	Zhang et al. [4]	2.5×10^{-4}		3.1 ± 0.4	–	3.4 ± 0.7

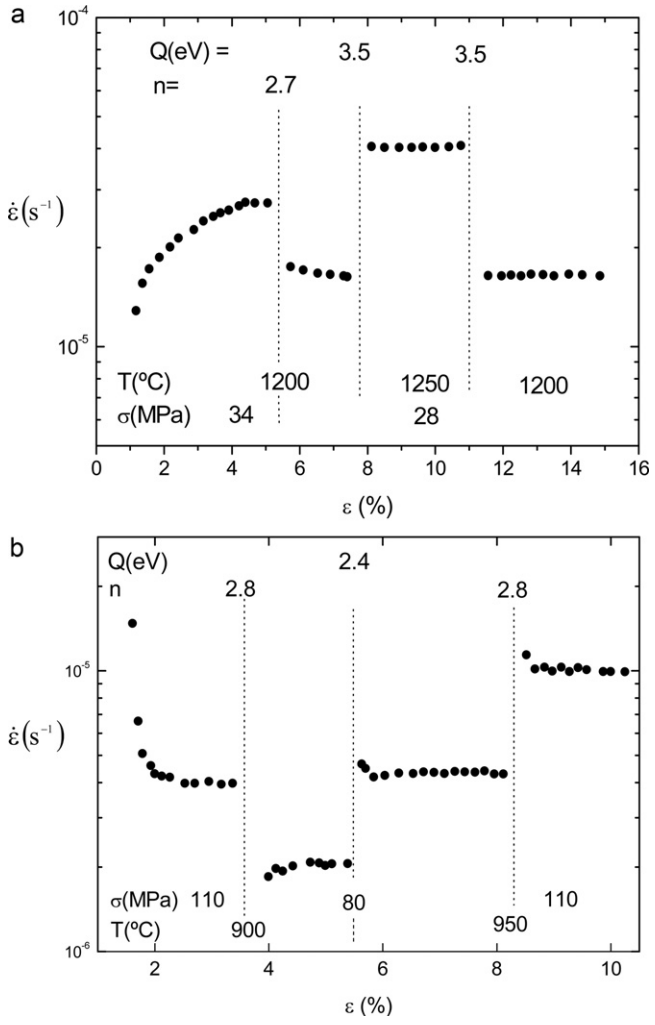

Fig. 4. Strain rate versus strain in the creep tests. The experimental conditions of the test and the calculated value of the creep parameters, n and Q, are indicated on the figure. (a) At temperatures $T > T_c$ and (b) at temperatures $T < T_c$.

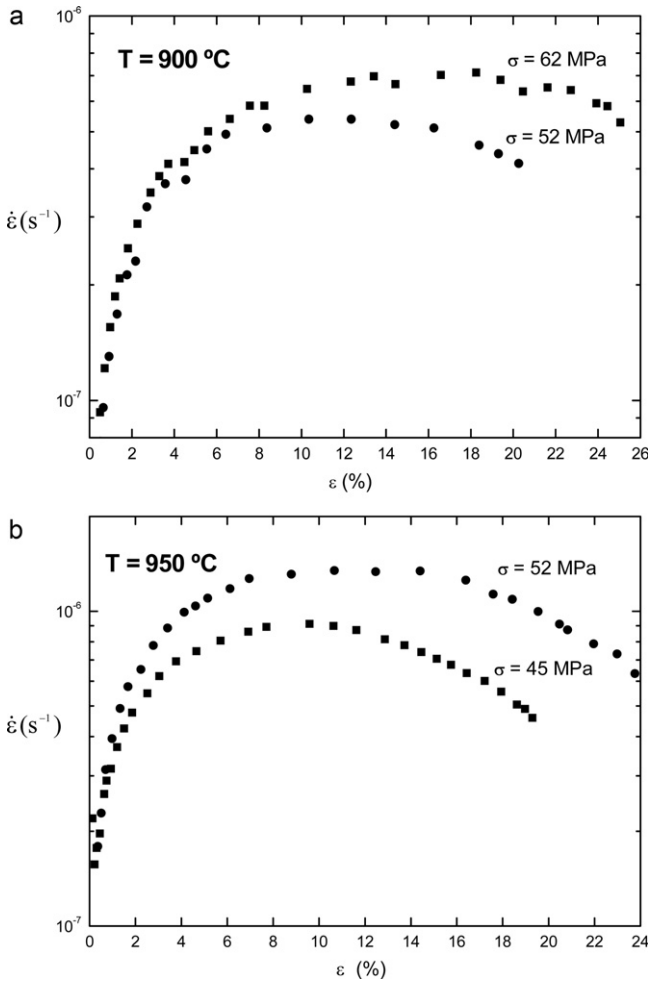

Fig. 5. Strain rate versus strain in the creep tests at $T < T_c$ and low stresses. (a) $T = 900$ °C and (b) $T = 950$ °C.

$T < T_c$, applying small stresses. Under these conditions the specimen deformed at a very low rate, avoiding the fracture of the material that could occur at higher strain rates. Fig. 5 shows the curves of strain rate versus strain for $T = 900$ °C and $T = 950$ °C and stresses between 45 and 62 MPa. Of note in these curves is the long initial transient regime in which the curves rise with increasing deformation ε. This long transient is indicative of the slowness with which the deformation mechanisms become activated at these low temperatures and stresses. One also notes that at high strains there is a slow decline in the strain rate, indicating a certain saturation of the deformation mechanism. From the creep curves of Fig. 5a and b at $\sigma = 52$ MPa, we obtained the deformation mechanism's activation energy as a function of the deformation. To this end, we used Eq. (5) with the assumption that the microstructure of the material depends only on the deformation ε and is not significantly affected by the temperature at which this deformation has taken place. Fig. 6 shows the results. The intercept of the best least squares straight line fit to these points gives an activation energy of $Q = 1.4 \pm 0.1$ eV which is within the range of values obtained previously for these temperatures. Table 3 summarizes the test conditions and the results of the different creep experiments.

3.3. Optical microscopy observations

With the activation of a glide system, there appear traces on the lateral faces of the specimen. These are the intersections of the glide planes with these faces whenever the direction of glide is not contained in the plane of these faces. To verify that the deformation of the specimens takes place by activation of a single system of basal glide of the type $(0\,0\,0\,1)(1/3)\langle\bar{1}\,2\,\bar{1}\,0\rangle$, observations were made under optical microscopy of the lateral faces of the specimens following the tests, measuring the angle between the glide planes and the compression axis on each face. On faces parallel to the plane $\{\bar{1}\,0\,1\,0\}$, there should appear traces forming 45° with the compression axis, and on faces perpendicular to the this plane the traces should be normal to that axis. With optical microscopy, these traces were observed for temperatures both above and below T_c (Fig. 7). While at temperatures below T_c the glide lines on the face parallel to the plane $\{\bar{1}\,0\,1\,0\}$ are very clear, even being visible to the naked eye (Fig. 7b), at temperatures above T_c they are very weak and

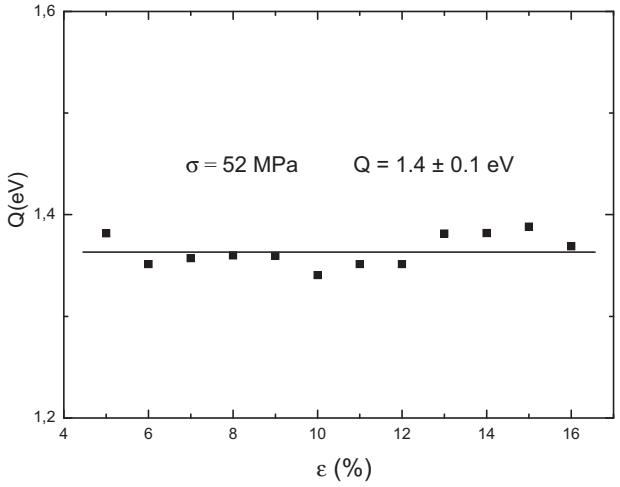

Fig. 6. Activation energy Q versus strain, obtained from the creep tests at $\sigma = 52$ MPa and temperatures of 900 °C and 950 °C (Fig. 5a and b) using Eq. (4).

difficult to observe (Fig. 7d). These observations indicate that, although in both cases the deformation occurs by basal dislocation glide, a different deformation mechanism is involved in each case. This is consistent with the results of the mechanical tests.

3.4. Transmission electron microscopy (TEM) observations

The TEM observations are of great help in correlating the mechanical test results with the material's dislocation microstructure. For information on the dislocation fine structure, observations were made using the weak beam technique. The micrographs obtained from deformed specimens at temperatures both above and below T_c show a microstructure in which the dislocation lines have long straight segments in simple crystal directions (Figs. 8 and 9). This microstructure is typical of the mechanism of pairs of kinks where the dislocation line is in Peierls valleys.

At temperatures above T_c and low strain rates (less than 6×10^{-5} s^{-1}), most basal dislocations appear dissociated into two very close partial dislocations (Fig. 8). The analysis of these dislocations by the **g**·**b** method shows that the dissociation takes place according to Eq. (1).

In contrast, at temperatures below T_c one observes (Fig. 9) that the dislocation lines are not doubled, indicating that either the dislocations are not dissociated or that it is a case of a partial whose twin is not within the viewing area. The **g**·**b** analysis of these dislocations shows that it is a single partial dislocation with a Burgers vector $(1/3)\langle\bar{1}\,1\,0\,0\rangle$. This may be the partial in Eq. (1) which glides first (leading) or that which follows (trailing), with its twin being far away and outside the viewing area, or it may be a case of a leading partial whose trailing twin has not nucleated.

Previous studies in semiconductors [14–16] have shown that the glide activation energy of the leading partial is lower than that of the trailing partial. Therefore, at low temperatures, if the applied stress is not great enough then the trailing partial may not begin to move at all, and the leading partial will glide alone, leaving behind a stacking fault. At higher temperatures, the thermal energy contribution will enable the activation of the trailing partial, allowing both the leading and the trailing partials to glide together like a perfect dislocation (albeit dissociated). The slip plane of these glide dislocations (g) is between the closest layers of C and Si atoms in the 4H–SiC structure. The two partials are different in nature [9]. The more mobile (leading) partial has a silicon core and corresponds to what is denominated the Si(g), while the less mobile (trailing) partial has a carbon core and corresponds to C(g). This different nature is the reason for the difference in their glide activation energy, and hence of their different mobilities. According to the Peierls model, the movement of the dislocations is a consequence of the nucleation and propagation of kink pairs, and both these processes require the rupture and reconstruction of bonds in new Peierls valleys (primary Peierls valleys for nucleation and secondary for propagation). These bonds are of the C–C type in C(g) and Si–Si type in Si(g). Since the Si–Si bond has a lower binding energy (~2.3 eV) than the C–C bond (~3.7 eV) [17], for the same applied resolved stress τ_c the kink pair can nucleate and propagate more easily in Si(g) than in C(g). Therefore, the activation energy of motion of the leading Si(g) partial will be lower than that of the trailing C(g) partial.

4. Discussion

As was noted above, for covalent crystals the experimentally determined dislocation strain rates agree well with Eq. (2). In particular, in high-purity crystals, values of n close to 3 have been found [18]. This value was also obtained theoretically by Hirth and Lothe [12] in the kink pairs model based on the Peierls mechanism for the movement of dislocations. The values of n obtained in the present work ($n = 2.8 \pm 0.8$ in tests at constant strain rate, and $n = 2.9 \pm 0.3$ in tests at constant load) suggest that it is the Peierls mechanism which controls the speed of the dislocations, and therefore the strain rate, in 4H–SiC. This was confirmed by the optical microscopy observations on the

Table 3
Conditions of the 4H–SiC creep tests, and values of the parameters n and Q determined in each case.

	$T < T_c$ (900–950 °C)		$T > T_c$ (1150–1250 °C)
	Low σ	High σ	
σ (MPa)	45–62	80–110	28–43
$\dot{\varepsilon}$(s^{-1})	5.0×10^{-7} to 2.0×10^{-6}	2.1×10^{-6} to 2.0×10^{-5}	7.5×10^{-6} to 7.8×10^{-5}
n	–	2.9 ± 0.3	2.9 ± 0.3
Q (eV)	1.4 ± 0.1	2.3 ± 0.6	3.5 ± 0.7

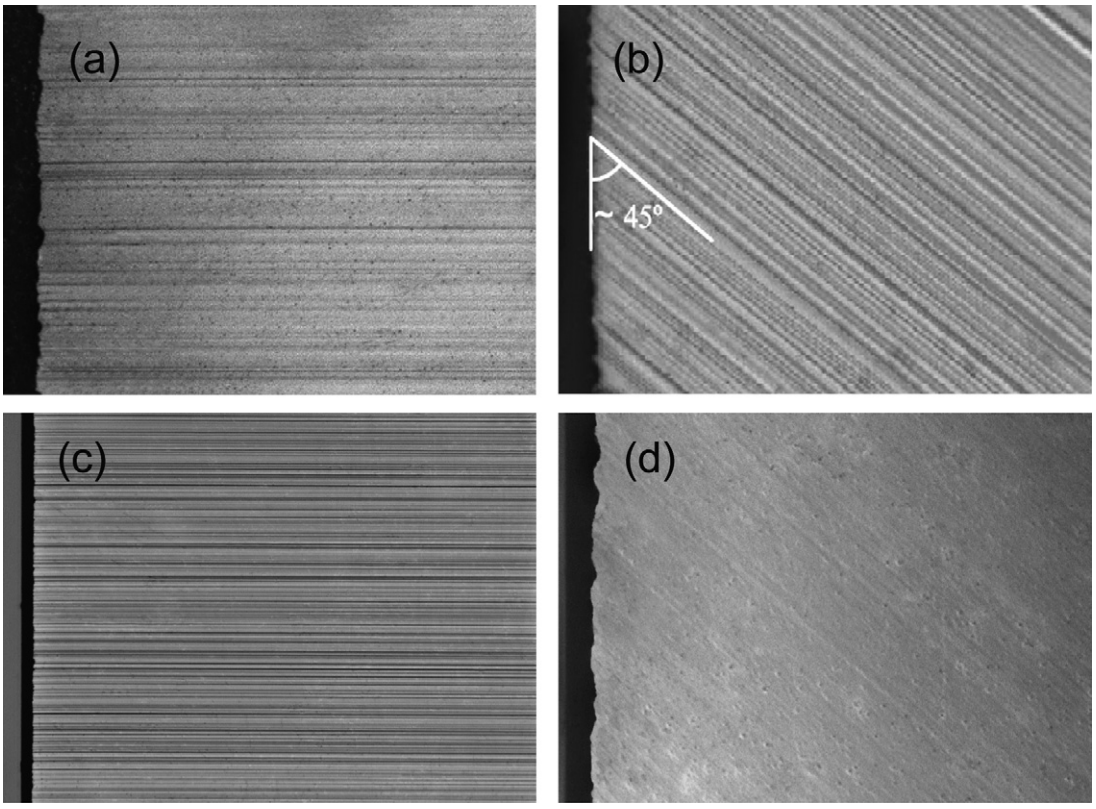

Fig. 7. Optical micrographs of the lateral faces of the deformed samples: (a) and (b) correspond, respectively, to the faces perpendicular and parallel to the plane $\{\bar{1}\,0\,1\,0\}$ of a sample tested at $T = 900\ ^{\circ}\mathrm{C}$ ($T < T_c$) and deformed to $\varepsilon = 11\%$; (c) and (d) correspond, respectively, to the faces perpendicular and parallel to the plane $\{\bar{1}\,0\,1\,0\}$ of a sample tested at $T = 1194\ ^{\circ}\mathrm{C}$ ($T > T_c$) and deformed to $\varepsilon = 8\%$.

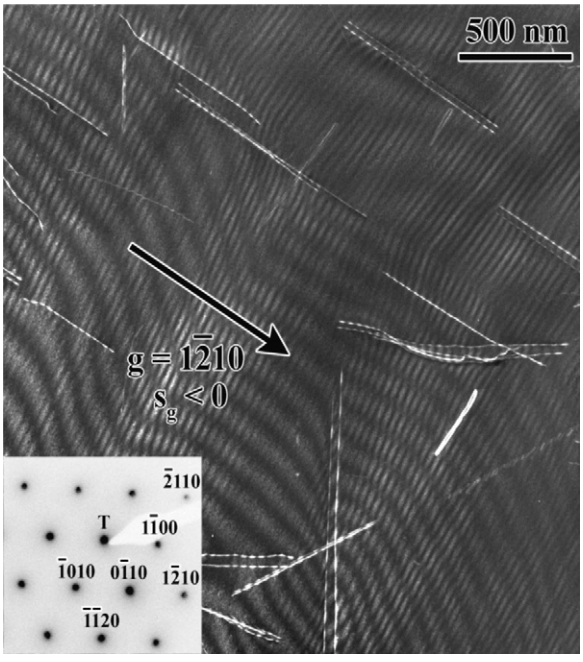

Fig. 8. TEM micrographs of the dislocation microstructure of a 4H–SiC specimen deformed by basal slip at $T = 1104\ ^{\circ}\mathrm{C}$. The foil is parallel to the basal plane. Most of the basal dislocations are dissociated into two partials, according to Eq. (1). Included is the diffraction diagram with the identification of the crystallographic directions.

lateral faces of the deformed specimens and by the transmission electron microscopy (TEM) observations. In the latter case, the micrographs (Figs. 8 and 9) show long straight traces in the simple crystal directions presented by the dislocation lines, a consequence of the high value of the Peierls barrier the dislocations have to surpass in order to glide. Other authors [4,7,19] have reported similar values of n (Table 2).

The change in slope of the plot of $\ln \tau_c$ versus $1/T$ at $T_c = 993\ ^{\circ}\mathrm{C}$ obtained in the present work is consistent with the fact that at low temperatures the applied stress only allows activation of the leading partial, so that it is the movement of this partial which is responsible for the deformation. The activation energy obtained in this case ($Q = 0.7 \pm 0.3$ eV in tests at constant strain rate, and Q between 1.4 ± 0.1 and 2.3 ± 0.6 eV in deformation tests at constant load) corresponds to the activation energy of motion of the Si(g) partial. Indeed, Rabier and George [2] report for the activation energy of motion of dislocations in Si single crystals a value of approximately 2 eV, and this value has to be close to that of the Si(g) partial in SiC since in both cases the activation energy is determined mainly by the energy of the Si–Si bonds that are broken and reconstructed in the movement of the dislocation. Other authors [6,7,19] have found values close to these for the activation energy of SiC at temperatures below T_c (Table 2).

For higher temperatures, $T > T_c$, thermal energy contributes to the rupture of the C–C bonds, allowing the nucleation and propagation of kink pairs in the C(g) partial. In this case, the

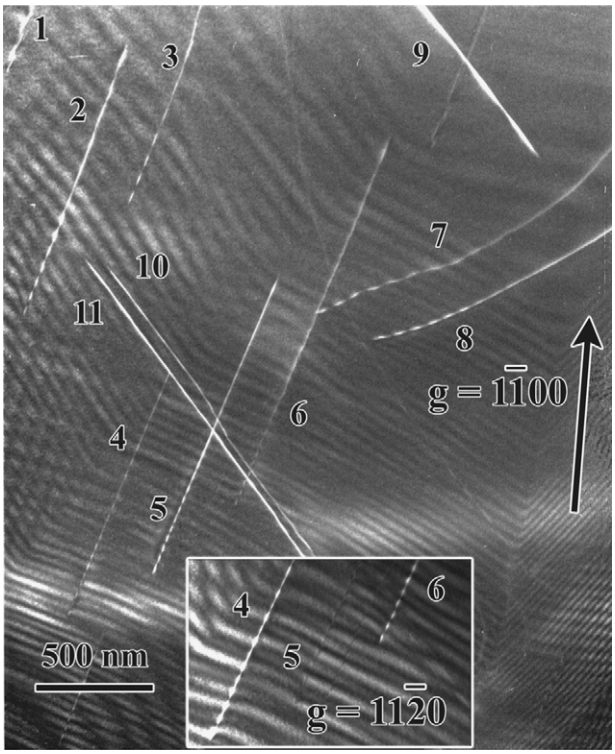

Fig. 9. TEM micrographs of the dislocation microstructure of a 4H–SiC specimen deformed by basal slip at $T = 900\ ^{\circ}C$. The foil is parallel to the basal plane. The dislocation segments labeled {1, 2, 6, 7}, {5, 9, 10, 11}, and {3, 4} have Burgers vectors $(1/3)[0\,1\,\bar{1}\,0]$, $(1/3)[\bar{1}\,1\,0\,0]$ and $(1/3)[1\,0\,\bar{1}\,0]$, respectively.

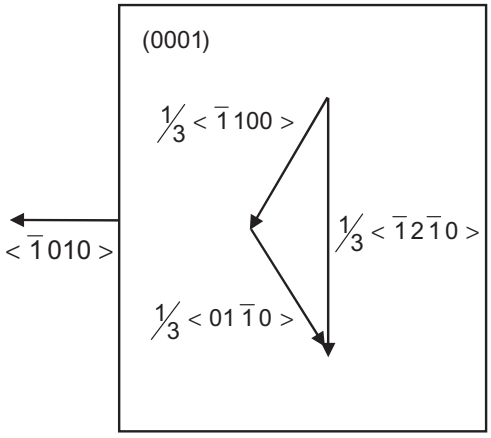

Fig. 10. Orientation relative to the lateral faces of the sample of the Burgers vectors of the perfect basal dislocation and the partial dislocations into which it is dissociated, according to Eq. (1).

two partials glide at the same time with a small separation between them, so that the C(g) partial eliminates the stacking fault left by the movement of the Si(g) partial, with this stacking fault being limited to the zone between the two partials. In this simultaneous movement of the two partials, the glide speed is determined by that of the less mobile, i.e., the C(g) partial. The deformation activation energy must in this case be that of the trailing partial, and therefore greater than that corresponding to $T < T_c$. This agrees well with the Q values obtained in the present work for $T > T_c$: $Q = 3.3 \pm 0.6$ eV at constant strain rate, and $Q = 3.5 \pm 0.7$ eV at constant load. Values close to these have been reported by other authors [4,6,7,19] for this temperature range (Table 2).

The TEM observations at $T < T_c$ (Fig. 9) show the presence of partial dislocations with Burgers vector $(1/3)\langle\bar{1}\,1\,0\,0\rangle$ whose twins are not in the viewing area. The deformation must therefore occur by the glide of this single partial, which leaves behind it a large stacking fault region observable in the micrographs. This is the leading Si(g) partial. At $T > T_c$, the TEM images (Fig. 8) show the presence of basal dislocations with Burgers vector $(1/3)\langle\bar{1}\,2\,\bar{1}\,0\rangle$ dissociated according to Eq. (1) into two very close leading/trailing partials, with a stacking fault between them. Optical microscopy of the lateral faces of the deformed specimens confirms the existence of this difference in deformation mechanism according to whether the test temperature is above or below T_c. In accordance with Eq. (1), Fig. 10 shows the orientation of the Burgers vectors of the basal dislocation and the corresponding partial dislocations relative to the specimen's lateral faces. At $T > T_c$, the two partial dislocations Si(g) and C(g) move simultaneously as a perfect dislocation, so that the glide of a basal relative to the contiguous plane takes place in the direction $\langle\bar{1}\,2\,\bar{1}\,0\rangle$, and therefore leaves no trace on the face parallel to the plane $\{\bar{1}\,0\,1\,0\}$. The weak traces that can be seen in some of these specimens (Fig. 7d) result from small deviations in their orientation. At $T < T_c$, only the partial dislocation associated with the silicon Si(g) moves. This partial glides in the direction $\langle\bar{1}\,1\,0\,0\rangle$, oblique to the face $\{\bar{1}\,0\,1\,0\}$, so that the movement of the basal plane relative to the contiguous should leave a trace on that face. These traces are very clear, even visible to the naked eye, in specimens deformed at $T < T_c$ (Fig. 7b).

At temperatures below T_c, the stacking fault left behind by the leading partial as it glides in the basal plane prevents the formation and movement in the same plane of a new partial of the same type generated by the same Frank-Read source [9]. For the source to be able to emit a new partial, it has to change plane through a mechanism of double cross-slip [20] to reach a new basal plane parallel to the previous one, in which it will be able to generate and emit a new partial. This mechanism is slow and therefore inefficient for achieving high strain rates, and requires a greater stress applied to the partials. As a consequence, in the mechanical tests at constant strain rate, the σ–ε curves at $T < T_c$ (Fig. 2) do not show the yield point which is generally found when the dislocation multiplication occurs under conditions in which they can all slide in the same plane without difficulty. In this case, there is no need for sharp drops in the applied stress to achieve the necessary readjustments of the glide speed of the dislocations to the strain rate imposed in the trials. Also, the slowness of the double cross-slip process in generating partial dislocations in parallel basal planes, especially for small applied stresses, means that a long time would be required for the activation of enough of these partials to allow the strain rate to reach significant values. This may be the reason for the long initial transient in the creep curves for very small stresses and temperatures below T_c (Fig. 5). Likewise, the work-hardening of the material observed

in these trials for high values of the deformation ε (manifest in the reduction of the strain rate $\dot{\varepsilon}$) may be a consequence of the saturation of the described deformation mechanism. Indeed, as the deformation of the material increases, there is a concomitant increase in the number of basal planes in which glide of the leading partial has taken place. This increases the difficulty the sources will face in finding, by means of a double cross-slip process, a new basal plane in which to emit a new partial that can glide without originating an excessively high stacking fault energy. Consequently, the material's strain rate must decrease for high deformation values (Fig. 5).

At $T > T_c$, the movement of the trailing partial eliminates the stacking fault left by the glide of the leading partial. The Frank-Read source is thus left operative to emit a new pair of partials in the same glide plane. Since any given source can emit many dislocations in the same glide plane, this constitutes a highly efficient mechanism for a major deformation of the crystal. In this temperature range, the material should present a ductile behaviour. On the contrary, the deformation mechanism described above for lower temperatures ($T < T_c$) is highly inefficient for the production of plastic deformation of the crystal. Consequently, in this temperature range, deformation is very restricted. If the strain rate imposed on the material by the experimental conditions surpasses the dislocation speed allowed by this relatively inefficient deformation mechanism, then fracture occurs. In this temperature range, the material will have a brittle behaviour. This interpretation is supported by the experimental results for the brittle–ductile transition temperature (T_{BDT}) in SiC. Thus, for 4H–SiC, Demenet et al. [7] obtain $T_{BDT} = 1030\ ^\circ C$ at $\dot{\varepsilon} = 2.6 \times 10^{-6}\ s^{-1}$ and $T_{BDT} = 1160\ ^\circ C$ at $\dot{\varepsilon} = 3.6 \times 10^{-4}\ s^{-1}$, and Zhang et al. [21] obtain $T_{BDT} = 1050\ ^\circ C$ at $\dot{\varepsilon} = 5.0 \times 10^{-7}\ s^{-1}$ and $T_{BDT} = 1185\ ^\circ C$ at $\dot{\varepsilon} = 4.0 \times 10^{-6}\ s^{-1}$. These values are in reasonable agreement with those obtained in the present work for T_c.

5. Conclusions

- The σ–ε curves obtained from the constant strain rate compression tests show a change in the mechanism controlling plasticity. An estimation of the transition temperature $T_c \sim 993\ ^\circ C$ has been obtained. For $T > T_c$ the value of the stress exponent $n = 2.8 \pm 0.8$ has been determined. For $T < T_c$, it was impossible to obtain n by change of the strain rate due to the fracture of the samples at the experimental conditions imposed by the test machine. At the same time, a change in the activation energy has also been found. The values $Q = 0.7 \pm 0.3$ eV, for $T < T_c$, and $Q = 3.3 \pm 0.6$ eV, for $T > T_c$ has been obtained.
- From the creep tests, the stress exponent $n = 2.9 \pm 0.3$ has been obtained for temperatures between 900 and 1250 °C. In addition, the activation energy has been determined in the different ranges of temperature. For $T < T_c$, the values $Q = 1.4 \pm 0.1$ eV and $Q = 2.3 \pm 0.6$ eV, at low and high stresses respectively, and for $T > T_c$, $Q = 3.5 \pm 0.7$ eV have been obtained.
- The TEM observations have allowed correlating the different mechanical behaviours of the material with the microstructure of dislocations responsible of the deformation. At temperatures higher than T_c most of the basal dislocations are dissociated into two partials that glide simultaneously with a small stacking fault between them. At temperatures lower than T_c, the deformation takes place by the glide of one of the partials, the one with lower activation energy – Si(g) partial – while the twin partial with higher activation energy – C(g) partial – has not been nucleated. The glide of the Si(g) partial leaves behind it a large stacking fault zone in the glide plane. The optic observations in the lateral faces of the deformed samples confirm the proposed mechanisms of deformation.
- The activation energies obtained in this study are consistent with the proposed mechanisms. At $T < T_c$, the glide of the Si(g) partial is responsible of the deformation, and the activation energy has to be determined by the energy of the Si–Si bonds (~2.3 eV) that has to be broken and reconstructed in the movement of the dislocation. For $T > T_c$, both partials glide at the same time and the speed is determined by the one with less mobility, i.e., the C(g) partial. In this case, the activation energy is determined by the energy of the C–C bonds (~3.7 eV).
- At $T < T_c$, the stacking fault left behind in the basal plane by the Si(g) partial prevents the formation and movement in the same plane of a new partial. In order that the source emits a new partial, it has to change its plane through a double cross-slip mechanism. This process of generation of partials is relatively slow, especially for low applied stresses. The long time required for the activation of a high number of partials has allowed explaining the most significant characteristics of the deformation of the material in this range of temperatures.

Acknowledgements

This work was financially supported by the Ministry of Education and Science (Government of Spain) through the project MAT 2006-03068 and by the Junta de Andalucía (Spain) through the excellency project P05-0337-F*Q*M.

References

[1] A. George, J. Rabier, Dislocations and plasticity in semiconductors. I – Dislocation structures and dynamics, Rev. Phys. Appl. 22 (1987) 941–966.
[2] J. Rabier, A. George, Dislocations and plasticity in semiconductors. II – The relation between dislocation dynamics and plastic deformation, Rev. Phys. Appl. 22 (1987) 1327–1351.
[3] Yu.M. Tairov, V.F. Tsvetkov, Investigation of growth process of ingots of silicon carbide single crystals, J. Cryst. Growth 43 (1978) 209–212.
[4] S. Fujita, K. Maeda, S. Hyodo, Dislocation glide motion in 6H–SiC single crystals subjecter to high-temperature deformation, Phil. Mag. A 55 (1987) 203–215.
[5] A.V. Samant, W.L. Zhou, P. Pirouz, Effect of test temperature and strain rate on the yield stress of monocrystalline 6H–SiC, Phys. Stat. Sol. 166 (1998) 155–169.
[6] A.V. Samant, P. Pirouz, Activation parameters for dislocation glide in α-SiC, Int. J. Refract. Met. Hard Mater 16 (1998) 277–289.
[7] J.L. Demenet, M.H. Hong, P. Pirouz, Plastic behaviour of 4H–SiC single crystals deformed at low strain rates, Scrip. Mater. 43 (2000) 865–870.
[8] J.L. Demenet, J. Radier, X. Milhet, M.H. Hong, P. Pirouz, I. Stretton, P.J. Cordier, Microstructures of 4H–SiC single crystals deformed under very high stresses, Phys. Condens. Matter 14 (2002) 12961–12966.

[9] P. Pirouz, J.W. Yang, Polytypic transformations in SiC: the role of TEM, Ultramicroscopy 51 (1993) 189–214.
[10] G.S. Corman, Creep of 6H α-silicon carbide single crystals, J. Am. Ceram. Soc. 75 (1992) 3421–3424.
[11] M.A. Meyers, K.K. Chawla, Mechanical Behaviour of Materials, Prentice Hall, New Jersey, 1999.
[12] J.P. Hirth, J. Lothe, Theory of Dislocations, Mc Graw Hill, New York, 1968.
[13] P. Pirouz, M. Zhang, J.L. Demenet, H.M. Hobgood, Yield and fracture properties of the wide and-gab semiconductor 4H–SiC, J. Appl. Phys. 93 (2003) 3279–3290.
[14] X.J. Ning, T. Perez, P. Pirouz, Indentation-induced dislocations and microtwins in GaSb and GaAs, Phil. Mag. A 72 (1995) 759–837.
[15] X.J. Ning, P. Pirouz, A large angle convergent beam electron diffraction study of the core nature of dislocations in 3C–SiC, J. Mater. Rev. 11 (1996) 884–894.
[16] X.J. Ning, N. Havey, P. Pirouz, Dislocation cores and hardness polarity of 4H–SiC, J. Am. Ceram. Soc. 80 (1997) 1645–1652.
[17] W. Lambrecht, O.K. Anderson, Minimal basis sets in the linear muffin-tin orbital method: application to the diamond-structure crystals C, Si, and Ge, Phys. Rev. B 34 (1986) 2439–2449.
[18] M. Imai, K. Sumino, In situ X-ray topographic study of the dislocation mobility in high-purity and impurity-doped silicon crystals, Phil. Mag. A 47 (1983) 599–621.
[19] A.V. Samant, M.H. Hong, P. Pirouz, The relationship between activation parameters and dislocation glide in 4H–SiC single crystals, Phys. Stat. Sol. 222 (2000) 75–93.
[20] K.P.D. Lagerlöf, J. Castaing, P. Pirouz, A.H. Heuer, Nucleation and growth of deformation twins: a perspective based on the double-cross-slip mechanism of deformation twinning, Phil. Mag. A 82 (2002) 2841–2854.
[21] M. Zhang, H.M. Hobgood, J.L. Demenet, P. Pirouz, Transition from brittle fracture to ductile behavior in 4H–SiC, J. Mater. Rev. 18 (2003) 1087–1095.